

KINEMATICS OF K GIANTS IN THE OUTER GALACTIC HALO

KAVAN U. RATNATUNGA¹ AND K. C. FREEMAN

Mount Stromlo and Siding Spring Observatories, Research School of Physical Sciences, Australian National University

Received 1984 August 6; accepted 1984 October 1

ABSTRACT

We describe a technique for finding field K giants in the outer galactic halo, 10–40 kpc from the galactic center. A sample of over 150 distant halo giants was located from an automated objective-prism survey of three high galactic latitude fields, each of 20 square degrees. Radial velocities of these giants show that (1) the outer halo is at most slowly rotating and (2) the line-of-sight velocity dispersion in our two best studied fields is approximately constant with distance from the Sun. However, the 60 km s^{-1} dispersion at the south galactic pole is much less than the 124 km s^{-1} dispersion in the SA 127 ($l = 272^\circ$, $b = 38^\circ$) field.

Our data on the run of velocity dispersion with distance in the halo fits well to a simple kinematical model in which the components (σ_R , σ_ϕ , σ_z) of the velocity dispersion in cylindrical polar coordinates (with origin at the galactic center) remain constant everywhere, and equal to the anisotropic values seen in the solar neighborhood. This model is also an excellent fit to Pier's data for blue horizontal-branch (BHB) stars in the inner halo. The corresponding spherical polar model, in which the velocity ellipsoid is everywhere constant and elongated toward the galactic center, is inconsistent with the data.

Subject headings: galaxies: Milky Way — galaxies: structure — radial velocities — stars: late-type — stars: Population II — stars: stellar dynamics

I. INTRODUCTION

The kinematics of the outer galactic halo, and the radial variations of metal abundance, are important astrophysical parameters for any theory of the formation and evolution of our Galaxy. However, models of the chemical and dynamical properties of the halo are only weakly constrained by present observational data. Detailed chemical and kinematical data for the halo come only from the halo stars in the solar neighborhood, which are distinguished from disk stars by their spectroscopic and kinematic properties rather than by their location. Most of our present knowledge about the large-scale properties of the galactic halo comes from the globular cluster system. Until now, small samples of RR Lyrae variables were the only field halo stars known beyond 10 kpc from the Sun.

However, it is by no means clear that the globular clusters and the halo field stars belong to the same dynamical system. For example, Hartwick (1983) showed that the velocity dispersion of 52 metal-weak halo giants (Bond 1980) is $(\sigma_R, \sigma_\phi, \sigma_z) = (140, 108, 55) \text{ km s}^{-1}$. The velocity dispersion of the nearby RR Lyrae stars (Woolley 1978) is also similarly anisotropic. This is in contrast to the globular cluster system, which appears to have an isotropic dispersion of about 118 km s^{-1} (Frenk and White 1980). The reality of this kinematical difference is fairly well established, but its origin remains unclear; it suggests that the globular clusters may not be reliable dynamical probes of the outer galactic halo.

An *in situ* sample of distant halo stars would probe directly the properties of the outer galactic halo, and allow us to relate them to the detailed properties of halo stars in the solar neighborhood. We would like to know whether the local velocity anisotropy extends into the outer halo, because the global behavior of the velocity ellipsoid is a very useful indicator of the dynamical state of the galactic halo. Further, the systemic rotation of the outer halo is of particular interest, because this may reflect the angular momentum of the outer protogalactic

material. The few stars of the outer halo, which are now passing through the solar neighborhood on highly eccentric orbits, are unlikely to give a reliable measure of this rotation. The globular cluster system has a systemic rotation of 60 km s^{-1} as shown by Frenk and White (1980) from radial velocity measurements. A similar analysis of velocities of distant halo stars would give an independent and astrophysically more reliable measure of the halo rotation.

What kind of stars should we chose for an *in situ* sample of the outer halo? First, they need to be intrinsically bright, so that they can be studied to great distances. Second, their existence should not depend on the chemical properties of the outer halo. This argues against the use of RR Lyrae stars (Woolley 1978; Saha 1984) and blue horizontal-branch (BHB) stars (Pier 1983) to study the halo, although these have given very useful information.

For these reasons field K giants have long been recognized as ideal halo probes (see Kraft 1979). However, finding them is not straightforward; broad-band photometry is unable to separate these distant halo giants efficiently from the much more numerous nearby disk dwarfs of similar apparent magnitude and color. This has made these halo giants elusive.

We have developed automated procedures to locate large *in situ* samples of field K giants in the outer halo and open these distant regions of our Galaxy for more detailed investigation. This is the first in a series of papers on the method and results of this survey. Slit spectroscopic observations of the sample are not yet complete. However, we believe that the kinematical results for the distant stars in two fields are sufficiently interesting to warrant their presentation at this time.

Section II describes the survey briefly. Section III contains details of the spectroscopic observations and analysis. The kinematical results are derived in § IV and discussed in § V.

II. SURVEY

A full description of the survey will be given in Ratnatunga (1984), and it is therefore only briefly discussed here.

¹ Now at Institute for Advanced Study, Princeton, NJ 08540.

We are interested in halo giants between about 5 and 40 kpc from the Sun. To reach these distances, we restrict the sample to giants with absolute magnitudes $M_v < 0.0$. These stars will have apparent magnitudes $13 < V < 18$, and colors $(B - V) > 0.7$. Since the nearby disk dwarfs in this range of color and magnitude greatly outnumber halo giants (by about 35:1 at the pole and more at lower latitudes), a very efficient procedure is required to separate the two populations.

Clark and McClure (1979) showed that the MgH + Mg *b* feature at 5100 Å is an excellent luminosity discriminant for stars in the limited color range $0.9 < (B - V) < 1.4$. The gravity-sensitive MgH band is strong in disk K dwarfs, while it is not seen in low-resolution spectra of metal weak K giants. Clark and McClure used intermediate band filters (an extension of the DDO system) to define a photometric Mg index. It seemed to us that this feature could be used successfully to separate halo giants from disk dwarfs with objective-prism spectra. A preliminary low-resolution (10 Å) slit spectroscopic survey of a complete sample of 126 red stars at the south galactic pole (SGP) (Bok and Basinski 1964), made with the Mount Stromlo Observatory 74 inch (1.9 m) telescope, confirmed the feasibility of this procedure (Ratnatunga 1982).

We have surveyed three high galactic latitude, 20 square degree Schmidt fields, designated by the selected areas which they include: SA 141 ($l = 240^\circ$, $b = -85^\circ$); SA 189 ($l = 277^\circ$, $b = -50^\circ$), and SA 127 ($l = 272^\circ$, $b = +38^\circ$). These fields were selected to give the radial and z velocity dispersions and also the mean rotation of the outer halo. To find the halo giant candidates, we first obtained photometry from direct *J* and *F* photographic plates taken for this survey by the United Kingdom Schmidt Telescope Unit (UKSTU) with the 48 inch (1.2 m) Schmidt Telescope. A complete catalog of photographic photometry for about 50,000 stars to a limiting apparent magnitude $V = 17.5$ was made from automated image analysis of PDS microdensitometer scans of these plates. The B_J and R_F magnitudes were transformed to B and V by means of transformations published by Carignan (1982). From comparison with the photometry of Bok and Basinski (1964) and Eriksson (1978) for a common sample of 400 stars at the SGP, the accuracy of our photometry is ± 0.04 mag in V and ± 0.06 mag in $(B - V)$ (s.e.).

This catalog of 50,000 stars contains about 5000 red stars with $(B - V) > 0.9$ and $13 < V < 16$. Luminosity classifications were made for these red stars from objective-prism plates taken for us by the European Southern Observatory on the 1 m Schmidt telescope at La Silla. The dispersion of the spectra is 450 \AA mm^{-1} at $H\gamma$. The wavelength range 4700–5400 Å, defined by a Schott GG 475 filter and the IIIa-J emulsion cutoff, was selected to classify the luminosity of these red stars from the MgH + Mg *b* feature. The classification used plots of digital spectra obtained after automated analysis of 2-dimensional PDS scans of individual objective-prism images. The resolution at Mg *b* is about 20 Å, which is ample to make the luminosity classification; it is also sufficient for us to be able to see the Mg *b* feature itself in the digital spectra of giants with $[\text{Fe}/\text{H}] > -1$. Examples of our objective-prism spectra are given by Ratnatunga and Freeman (1983).

The spectra of our red stars fell into three well-defined classes. About 90% of the spectra showed a strong MgH feature: these stars are the disk dwarfs. About 3% showed no MgH or Mg *b* feature: these are almost all metal-weak giants. We found a total of over 150 of these distant field K giants in the 60 square degrees surveyed. The third class shows no MgH,

but a distinct Mg *b* feature is visible: these are mostly relatively metal-rich giants ($[\text{Fe}/\text{H}] > -1$), with a possible contamination of dwarfs among the stars with $(B - V) \approx 0.9$, where the MgH luminosity criterion is breaking down.

III. OBSERVATIONS

We are now acquiring medium-resolution (2 Å) spectra of the giants selected by our survey, using the Anglo-Australian Telescope (AAT) with the RGO spectrograph and the IPCS, and the MSO 1.9 m telescope with the Boller and Chivens spectrograph and the 2-dimensional photon counting array (2DPCA). We have concentrated on the metal-weak giants. Our spectroscopic observations of metal weak giants in SA 141 and SA 127 are now more or less complete. Results for the more metal-strong giants are less advanced; they will be presented elsewhere.

Almost all of the stars observed were confirmed to be giants. We compared the Sr II $\lambda 4078$ and the Fe I $\lambda 4064$ lines. In K giants the Sr II line is stronger, while in dwarfs of similar temperature the Fe I line is much stronger (Morgan, Keenan, and Kellman 1943). Our spectra show these lines clearly, even for metal-weak stars. This higher resolution luminosity criterion removed any remaining dwarf contamination from the sample selected from objective-prism spectra. The contamination was found to be less than 5% and mainly among stars with $(B - V) \approx 0.9$, since the MgH feature used in the classification is weak in these hotter G dwarfs.

Radial velocities for the stars were determined using standard procedures (for details see Ratnatunga 1983), by cross-correlating the observations in the Fourier domain with a template generated by the sum of all the wavelength-calibrated observations. The zero point of our velocity system comes from observations of stars in 47 Tuc and ω Cen, for which unpublished velocities, accurate to 2 km s^{-1} , have been measured previously by Freeman. The AAT-IPCS spectra covered the wavelength range 3650–5450 Å. The interval 4410–5210 Å was used to measure the radial velocity from these observations. The MSO-2DPCA spectra covered the wavelength range 3600–4600 Å. The interval 4065–4275 Å was used for the radial velocity measurement. Table 1 gives the heliocentric radial velocities V_{rad} .

To estimate the abundances and then the distances, accurate photometry is needed. Photoelectric B , V observations have been made for the stars observed spectroscopically, using the Siding Spring Observatory 40 inch (1 m) telescope and the 2 channel chopping photometer. Since reddening in these high galactic latitude fields is expected to be small, we used the values determined by Burstein and Heiles (1982).

Since the sample is metal-weak, the Ca II H and K absorption lines were used to estimate the metal abundance. The calcium index $A(\text{Ca})$ (Norris and Freeman 1983) was calibrated as a function of metal abundance and $(B - V)$ color from similar observations of stars in a number of well-studied globular clusters, 47 Tuc ($[\text{Fe}/\text{H}] = -0.7$: Norris, Freeman, and Da Costa 1983), NGC 6752 ($[\text{Fe}/\text{H}] = -1.5$: Norris *et al.* 1981), and NGC 6397 ($[\text{Fe}/\text{H}] = -2.2$: Norris and Zinn 1977), and also of two metal-weak field halo stars, HD 122563 ($[\text{Fe}/\text{H}] = -2.7$: Norris 1983) and CD $-38^\circ 245$ ($[\text{Fe}/\text{H}] = -4.5$: Bessell and Norris 1984), with independent abundance estimates. Metal abundances measured for our field K giants covered the range seen in globular clusters, with mean metal abundance $[\text{Fe}/\text{H}] \approx -1.5$.

Absolute magnitudes M_p of the giants were determined from

TABLE 1
 OBSERVATIONS OF FIELD HALO K GIANTS

Identity	<i>l</i>	<i>b</i>	<i>V</i>	(<i>B</i> - <i>V</i>)	<i>M_v</i>	[<i>Fe</i> / <i>H</i>]	<i>d</i> kpc	<i>V_{rad}</i> km s ⁻¹	observation
SA141 $E(B-V) = 0.00$									
-290105 E	244.2	-85.0	13.58	0.91	0.2	-1.3	4.8	-27	101882 AAT
-300100 A	256.5	-85.9	14.42	1.35	-2.6	-2.1	25.1	-23	101882 AAT
-290100 C	252.5	-86.7	15.27	1.10	-2.3	-2.3	32.9	-66	101882 AAT
-300100 B	251.8	-85.7	15.59	1.04	-1.0	-1.4	20.6	-18	101882 AAT
-310115 C	248.8	-82.2	15.96	0.99	-0.4	-1.3	18.8	-39	101882 AAT
-320100 A	275.4	-84.7	15.71	1.03	-1.6	-1.9	28.7	-67	101882 AAT
-300105 F	253.1	-84.8	15.29	0.91	-0.6	-1.8	15.2	-39	101882 AAT
-300100 A	262.7	-85.9	15.08	1.27	-1.7	-1.4	22.7	0	101882 AAT
-300105 C	252.6	-84.8	14.90	0.86	-0.1	-1.6	9.9	-5	101882 AAT
-290105 B	236.0	-85.7	13.48	0.96	-0.8	-1.6	7.1	61	101882 AAT
-290105 G	241.7	-85.6	13.92	0.91	-0.1	-1.4	6.4	80	101882 AAT
-300105 A	250.4	-85.6	13.64	0.99	-0.6	-1.4	7.1	-33	101882 AAT
-310100 A	262.8	-85.2	13.22	1.07	-1.8	-1.9	9.9	37	101882 AAT
-300115 B	245.2	-83.3	13.24	1.23	-2.6	-2.3	14.5	88	101882 AAT
-300100 J	266.7	-85.5	14.01	0.95	-0.5	-1.5	8.1	-21	101882 AAT
-280100 A	231.4	-87.2	14.38	1.07	-0.9	-1.3	11.4	116	101882 AAT
-310110 A	250.4	-83.4	14.19	0.95	-0.2	-1.3	7.7	54	101882 AAT
-290105 J	244.3	-85.0	14.02	1.23	-1.1	-1.1	10.5	108	091182 MSO
-290105 C	243.2	-85.0	15.31	0.98	0.0	-1.1	11.6	59	091182 MSO
-290110 C	241.6	-84.2	13.28	1.16	-1.0	-1.2	7.3	-146	091282 MSO
-290055 H	255.9	-87.2	14.77	0.92	-0.1	-1.4	9.3	33	101182 MSO
-290105 N	238.5	-84.9	14.42	1.08	-1.3	-1.5	13.8	11	101182 MSO
-290055 C	257.4	-86.8	14.40	1.07	-2.0	-2.1	19.2	30	101182 MSO
-310100 H	249.3	-82.7	14.46	1.02	-0.6	-1.3	10.1	-2	101382 MSO
-310115 A	220.2	-84.1	15.72	1.04	-0.3	-1.0	15.8	-16	10783 AAT
-310105 H	256.5	-84.1	15.27	0.92	-0.3	-1.5	13.0	-40	110783 AAT
-310106 C	270.5	-85.4	15.22	0.93	-0.3	-1.5	12.6	20	110783 AAT
-290110 D	235.9	-84.0	15.52	1.01	0.1	-0.9	12.2	173	110783 AAT
-300110 C	245.3	-85.5	15.09	0.84	1.4	-0.9	5.4	88	110783 AAT
-300105 F	253.1	-84.8	15.29	0.91	-0.3	-1.5	13.2	-45	110783 AAT
-300115 A	240.0	-82.6	15.69	1.10	-1.0	-1.3	22.1	3	110783 AAT
SA189 $E(B-V) = 0.00$									
-590310 B	275.5	-49.9	13.69	1.06	-0.9	-1.3	8.3	35	101882 AAT
-600320 D	275.9	-47.4	13.79	0.98	-1.0	-1.7	9.0	-5	101882 AAT
-610320 E	273.5	-50.2	15.37	1.09	-1.4	-1.6	23.0	-12	101882 AAT
-610320 C	276.7	-47.8	13.30	1.19	-1.6	-1.5	9.6	119	101882 AAT
-600300 C	277.7	-50.4	13.47	0.83	0.5	-1.5	3.9	51	101882 AAT
-590300 H	277.4	-50.5	13.45	0.94	-0.2	-1.4	5.4	-9	101882 AAT
-580310 H	273.2	-49.7	13.44	1.04	-0.9	-1.4	7.4	51	101882 AAT
-590300 C	277.2	-50.6	13.92	1.01	-1.1	-1.7	10.3	41	101882 AAT
-580250 E	277.8	-52.1	13.37	0.90	1.1	-0.8	2.8	-29	090982 MSO
-590250 F	279.1	-51.5	13.80	1.02	-1.5	-1.9	11.5	-63	090982 MSO
-610320 E	276.4	-47.3	13.88	0.96	-1.1	-1.9	9.9	75	090982 MSO
-600320 A	275.7	-47.1	13.39	1.03	0.4	-0.7	3.9	1	101382 MSO
-580310 A	274.0	-49.3	15.07	0.97	0.0	-1.1	10.4	101	110783 AAT
-590300 D	277.4	-50.6	15.02	0.95	-0.5	-1.5	12.8	91	110783 AAT
-580250 G	276.1	-52.1	15.74	0.97	-1.3	-2.0	25.8	50	110783 AAT
-600250 M	278.6	-51.0	15.56	1.21	-1.0	-1.1	20.7	76	110783 AAT
-600320 L	274.8	-47.7	15.30	0.98	-0.9	-1.7	17.7	323	110783 AAT
-580300 D	274.7	-50.9	15.16	1.00	-1.4	-1.9	20.5	38	110783 AAT
-610250 G	281.3	-50.1	15.97	0.96	0.5	-0.9	12.4	161	110783 AAT
SA127 $E(B-V) = 0.03$									
-161110 B	272.6	40.2	13.98	1.22	-1.5	-1.5	12.0	227	031083 AAT
-191110 D	273.5	37.9	13.91	1.07	-1.2	-1.6	10.1	277	031083 AAT
-171105 A	271.6	39.1	14.80	1.49	-2.4	-1.6	27.3	210	031083 AAT
-181055 A	270.1	36.9	15.09	1.32	-1.7	-1.4	22.1	261	031083 AAT
-171115 A	274.8	40.1	14.89	1.22	-1.7	-1.6	19.9	210	031083 AAT
-181115 A	275.0	39.7	14.45	1.33	-2.5	-2.1	23.5	79	031083 AAT
-191110 E	273.5	37.7	14.68	1.29	-2.4	-2.0	24.7	293	031083 AAT
-171100 D	270.2	38.2	15.20	1.20	-2.0	-1.9	27.0	68	031083 AAT
-191105 B	272.5	36.7	14.94	1.09	-0.6	-1.1	12.3	-48	031083 AAT
-191105 C	272.2	36.8	14.34	1.34	-2.7	-2.3	24.2	231	031083 AAT
-171100 E	274.3	38.1	14.83	1.32	-2.2	-1.9	24.7	264	031083 AAT
-171100 A	270.9	38.3	15.33	1.09	-1.6	-1.8	23.3	285	031083 AAT
-191115 D	274.8	38.3	14.72	1.29	-1.1	-1.0	13.9	144	031083 AAT
-191110 A	274.3	38.0	15.79	1.29	-2.3	-2.0	40.7	61	031083 AAT
-171100 I	270.8	38.0	15.65	1.23	0.2	-0.4	11.9	88	031083 AAT
-161115 C	273.6	40.5	15.76	1.05	0.2	-0.9	12.6	253	031083 AAT
-161110 D	271.8	40.5	15.59	1.08	-0.6	-1.2	17.0	-52	031083 AAT
-161110 A	272.7	40.3	15.24	1.06	-0.8	-1.3	15.3	13	031083 AAT
-171100 H	269.7	37.6	15.14	1.05	-1.5	-1.9	20.3	107	031083 AAT
-191110 C	273.7	37.7	14.98	1.18	-1.5	-1.5	19.0	249	031083 AAT
-171115 E	274.0	39.5	15.61	0.93	-0.9	-2.0	19.3	188	031083 AAT
-161100 C	269.7	38.7	15.37	0.96	-0.3	-1.5	13.0	-11	031083 AAT
-161100 A	269.2	38.6	15.11	1.29	-1.7	-1.4	21.8	-4	031083 AAT
-181100 A	271.1	38.0	15.02	1.06	-0.5	-1.2	12.4	297	031083 AAT
-181100 B	271.3	37.7	15.08	1.03	-0.9	-1.5	14.8	84	031083 AAT
-191055 A	270.9	35.8	14.74	1.00	-0.3	-1.3	9.7	125	031083 AAT
-161105 E	270.5	39.1	15.46	0.97	-1.3	-2.1	21.2	281	031083 AAT
-171105 H	271.8	38.6	15.22	0.92	0.6	-1.1	7.9	-43	031083 AAT
-171105 I	271.7	38.6	15.10	0.99	-0.4	-1.4	12.0	-75	031083 AAT
-171110 F	272.1	39.6	15.51	0.99	0.2	-1.1	11.0	7	031083 AAT
-181105 K	272.7	38.1	15.43	0.97	-1.1	-2.0	19.7	369	031083 AAT
-161115 A	274.2	40.8	14.61	1.19	0.7	-0.3	5.9	30	031183 MSO
-161115 B	273.9	40.8	14.35	1.09	1.0	-0.3	4.4	296	031183 MSO
-161110 F	272.6	40.4	13.72	1.13	-0.1	-0.8	5.5	92	031183 MSO
-161110 C	271.8	40.5	13.63	1.05	0.3	-0.8	4.5	-36	031183 MSO
-191115 B	275.2	38.5	14.62	1.06	-0.4	-1.1	9.7	46	031183 MSO
-161105 A	271.0	39.7	14.54	1.07	-0.7	-1.3	10.7	102	031183 MSO
-161110 E	271.7	40.4	13.79	1.04	1.3	-0.4	3.1	256	031183 MSO
-191115 A	275.6	38.8	14.12	1.16	0.6	-0.4	4.8	82	031183 MSO

the $(B-V)_0$ color and estimated abundance $[\text{Fe}/\text{H}]$, by interpolation in a grid of observed globular cluster giant branches at different metal abundance. Any age-dependence of this calibration was assumed to be small compared with other uncertainties; the halo giants are assumed to be of similar age to the globular clusters. The distance d from the Sun to the star is then calculated directly from the observed apparent magnitude V , the absolute magnitude estimate M_v , and the adopted reddening $E(B-V)$.

The results of the estimates are given in Table 1 for all the halo giants measured by us so far. The stars tabulated are not a complete sample, since many halo giants located in the survey remain to be observed spectroscopically. Coordinate and finding charts will be published elsewhere.

For each star, the standard errors of the derived quantities $[\text{Fe}/\text{H}]$ and distance were estimated, including both observational errors and the intrinsic dispersions in the calibrations. These individual errors are not tabulated but are shown in the relevant figures. The error estimates used for this calculation are as follows: $(B-V)$, ± 0.02 mag; V , ± 0.03 mag; $E(B-V)$, ± 0.01 mag; $A(\text{Ca})$, ± 0.02 mag; intrinsic dispersion of $[\text{Fe}/\text{H}]$ calibration, ± 0.15 dex; and intrinsic dispersion of M_v calibration, ± 0.20 mag. The cumulative errors in the resulting estimates were typically ± 0.3 dex in $[\text{Fe}/\text{H}]$, ± 0.5 mag in M_v , and $\pm 20\%$ in distance d from the Sun. The error in the radial velocity was estimated from the observed scatter in the velocity estimates of the local velocity standards measured many times over each observing run. The typical error was ± 10 km s $^{-1}$ for the AAT observations and ± 15 km s $^{-1}$ for the MSO observations.

Although we observed only those giants which appeared metal-weak from their objective-prism spectra, a small number of relatively metal-rich ($[\text{Fe}/\text{H}] > -1$) giants have crept into our sample (see Table 1). We have not excluded these few stars from the kinematical discussion in this paper, because their kinematics appear similar to those of the more metal-weak stars; see Figure 1 for the two best observed fields, SA 141 and SA 127.

Table 2 gives the number of giants, the mean distance (d), mean height (z) above the galactic plane, mean abundance, mean radial velocity V_{los} (corrected for the Sun's peculiar motion relative to the LSR), and the line-of-sight velocity dispersion σ_{los} , for all stars and separately for stars at heights

below and above 10 kpc from the galactic plane. Figure 2 illustrates the variation of the corrected radial velocity with distance from the Sun for these stars. The range of distance is limited by the apparent magnitude and color limits of the survey: $13 < V < 16$ and $(B-V) > 0.9$. The differences in the mean velocity and the line-of-sight velocity dispersion in the two fields are clearly seen.

IV. ANALYSIS

a) SA 141 and SA 127

The analysis of the abundance distribution in the halo will be possible only after our complete sample has been observed spectroscopically; so far, we have concentrated our observations on the more metal-weak giants. Kinematically, however, we see no significant variations with abundance in our sample. Therefore, this initial subsample of mainly metal-weak giants gives a preliminary view of the halo kinematics that is unlikely to change significantly when the complete sample has been observed.

From Table 2, the mean velocity for stars at the SGP (SA 141) is near zero, as expected. For SA 127 the mean velocity of the more distant stars at $b = +38^\circ$ toward antirotation ($l = 270^\circ$) is about 178 ± 29 km s $^{-1}$, as could be expected for a stellar population that has low mean rotation. There are insufficient observations in the SA 189 field to imply that the measured mean of 83 ± 59 km s $^{-1}$ is significantly different from the value 140 km s $^{-1}$ expected for a population that has zero rotation (assuming $V_{\text{LSR}} = 220$ km s $^{-1}$).

The most significant difference between the SGP field and the high galactic latitude field SA 127 is the difference in velocity dispersion. The line-of-sight velocity dispersion for SA 127 is seen to be almost independent of distance, and is 114 ± 20 km s $^{-1}$ for 17 giants with a mean distance of 23 kpc. The velocity dispersion for the metal-weak stars at the SGP is again almost independent of distance. However, its value is much smaller (63 ± 10 km s $^{-1}$) for the 22 stars with a mean distance of 18 kpc.

This is a striking result, for the following reason. Let $R_\odot = 8.5$ kpc be the solar-galactocentric distance. The fields surveyed are practically on the plane normal to the galactic center-Sun line. At distances from the Sun $d \gg R_\odot$, the radial velocity measures mainly the (spherical polar) radial component of the star's motion relative to the galactic center. Therefore, at these large distances, we would expect the measured line-of-sight dispersions σ_{los} in both fields to be close to the radial component σ_r of the velocity ellipsoid. Now assume the velocity ellipsoid to be *spatially* spherically symmetric (i.e., its components depend only on spherical r , but without any further restriction on radial variation or anisotropy); we would then expect σ_{los} to be approximately equal in both fields. However, the large difference observed for the velocity dispersions in these two fields shows that the halo is kinematically far from spherically symmetric (in the above sense), at least within 25 kpc from the center. It also suggests that the velocity distribution of distant halo stars is as anisotropic as in the solar neighborhood. One might have expected that, at such large distances from the disk, the velocity dispersion in the halo would be more or less isotropic, as observed for the globular clusters, and spherically symmetric in the above sense. However, it now seems clear that the kinematics of the outer galactic halo cannot be represented by a spatially spherically symmetric galaxy model.

TABLE 2
MEAN KINEMATICS

Sub-sample	No. of Giants	$\langle d \rangle$ (kpc)	$\langle z \rangle$ (kpc)	$\langle [\text{Fe}/\text{H}] \rangle$	$\langle V_{\text{los}} \rangle$ (km s $^{-1}$)	σ_{los} (km s $^{-1}$)
SA 141 ($l = 240^\circ, b = -85^\circ 0'$)						
All	34	13.6	13.9	-1.5	3 ± 11	60 ± 8
$z < 10$	12	7.4	7.3	-1.4	11 ± 17	55 ± 12
$z > 10$	22	17.5	17.5	-1.5	-1 ± 14	63 ± 10
SA 189 ($l = 277^\circ 0', b = -50^\circ 0'$)						
All	19	12.5	9.6	-1.5	53 ± 19	81 ± 14
$z < 10$	14	8.7	6.6	-1.4	41 ± 16	56 ± 11
$z > 10$	5	21.5	16.6	-1.7	83 ± 59	117 ± 42
SA 127 ($l = 270^\circ 0', b = +38^\circ 6'$)						
All	39	17.0	10.6	-1.4	135 ± 20	124 ± 14
$z < 10$	22	10.9	6.8	-1.1	94 ± 26	120 ± 19
$z > 10$	17	23.3	14.5	-1.8	178 ± 29	114 ± 20

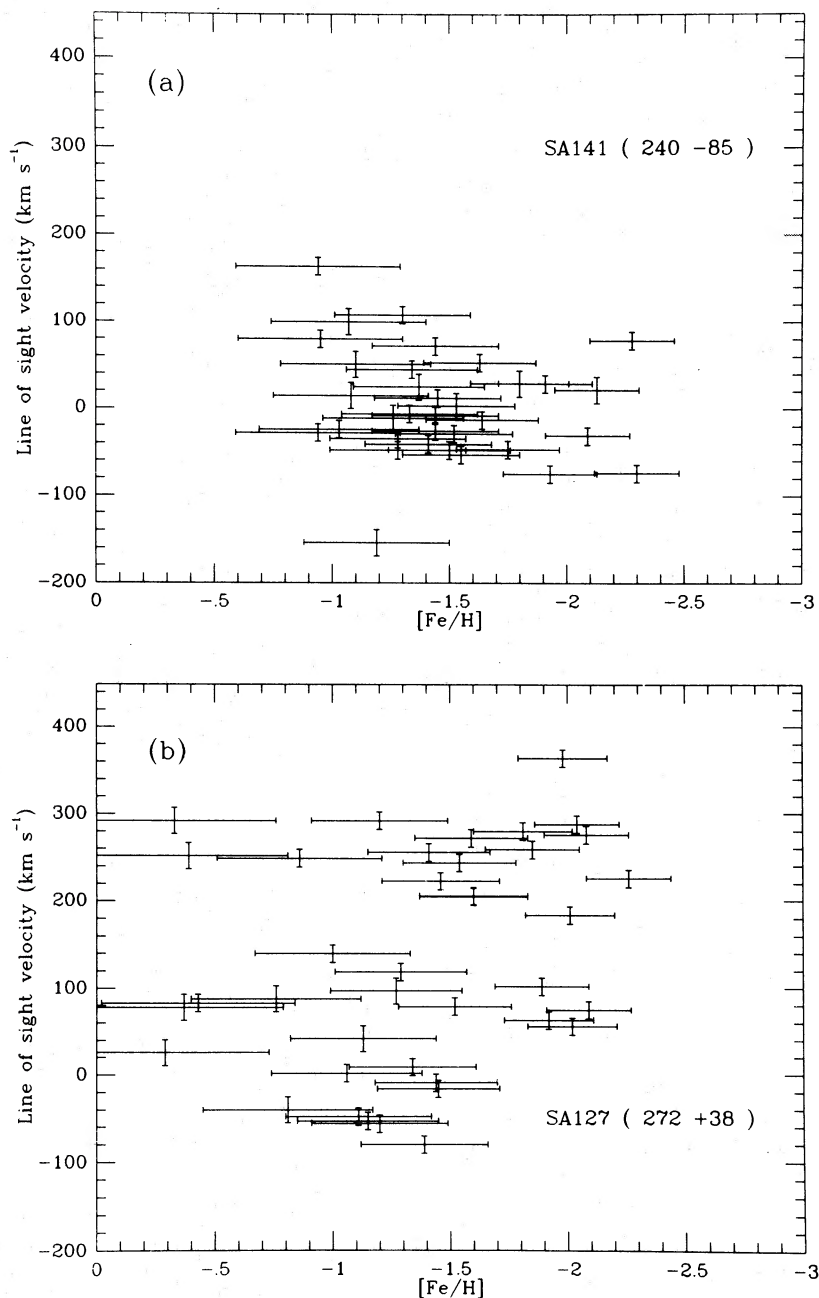


FIG. 1.—Line-of-sight velocity vs. $[Fe/H]$. The distribution shows no significant variation of velocity with abundance for the halo K giants in our fields (a) SA 141 (SGP) and (b) SA 127 ($l = 272^\circ$, $b = +38^\circ$).

For any axisymmetric system whose phase-space distribution function depends only on the two “classical” integrals of motion, energy and the component of angular momentum about the symmetry axis, the velocity dispersions in the radial and z -directions must be equal (Jeans 1916). The anisotropy observed in the solar neighborhood, and strongly suggested by our observations for the outer halo, requires galaxy models with a third integral. It is interesting to note that the scale-free model of Richstone (1980) has a velocity ellipsoid which is elongated toward the axis of symmetry as our data suggest. Realistic dynamical models will require specific information about the shape and orientation of the velocity ellipsoid; for this purpose, we now attempt to give a simple empirical

description of the velocity ellipsoid information derived from our observations, from the solar neighborhood, and from Pier’s (1982, 1983) data for BHB stars in the inner halo.

b) A Simple Working Picture

We will test the simple hypotheses that the velocity dispersion components are everywhere constant (but not equal), first in spherical polar coordinates with origin at the galactic center and then in cylindrical polar coordinates. In the discussion below, we will refer to these two cases as the spherical and the cylindrical hypotheses.

Consider now the usual spherical (r, ϕ, θ) and cylindrical (R, ϕ, z) polar coordinate systems, with origin at the galactic

center. The angle ϕ is in the direction of galactic rotation. The colatitude θ is measured from the Galaxy's north pole, and z is positive toward this pole. With our hypothesis of constant velocity dispersion components, we can calculate the expected run of σ_{los} with distance for any galactic longitude and latitude (l, b). For the spherical hypothesis we assume that $(\sigma_r, \sigma_\phi, \sigma_\theta)$ have everywhere the values (140, 108, 55) km s^{-1} derived by Hartwick (1983) for the solar neighborhood metal-weak giants. Similarly, for the cylindrical hypothesis, we assume that $(\sigma_R, \sigma_\phi, \sigma_z) = (140, 108, 55) \text{ km s}^{-1}$ everywhere. The predicted runs of σ_{los} for our two fields in these two cases are shown in Figure

3. For the SGP field in particular, the two cases are very different. This emphasizes the obvious point that kinematical data away from the galactic plane are needed to distinguish between the spherical and cylindrical hypotheses.

We now compare these predicted runs of σ_{los} with our observations. Velocity dispersion values were generated at mean distances separated by about 5 kpc, in the following way. At each nominal distance we include all stars at $\pm 40\%$ of this distance, and derive the true mean distance and dispersion for this subsample. For SA 141, we assume that the mean velocity for each subsample is zero, so the dispersions shown in Figure

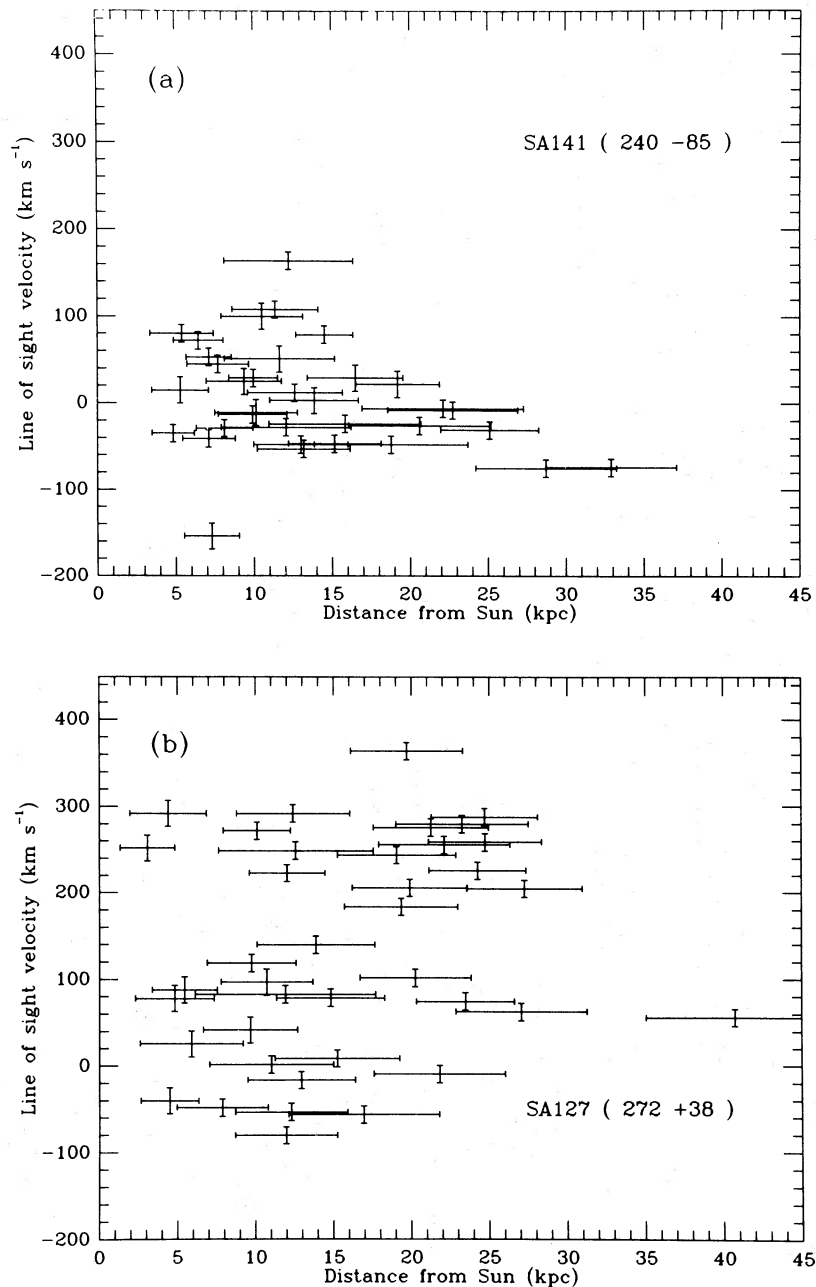


FIG. 2.—Line-of-sight velocities (corrected for the Sun's peculiar motion) of all the halo K giants observed in our fields (a) SA 141 and (b) SA 127 are shown plotted against their estimated distance from the Sun. Note in particular the high velocity dispersion in SA 127, compared with the much lower dispersion in the SGP field SA 141, and also the higher mean motion in SA 127.

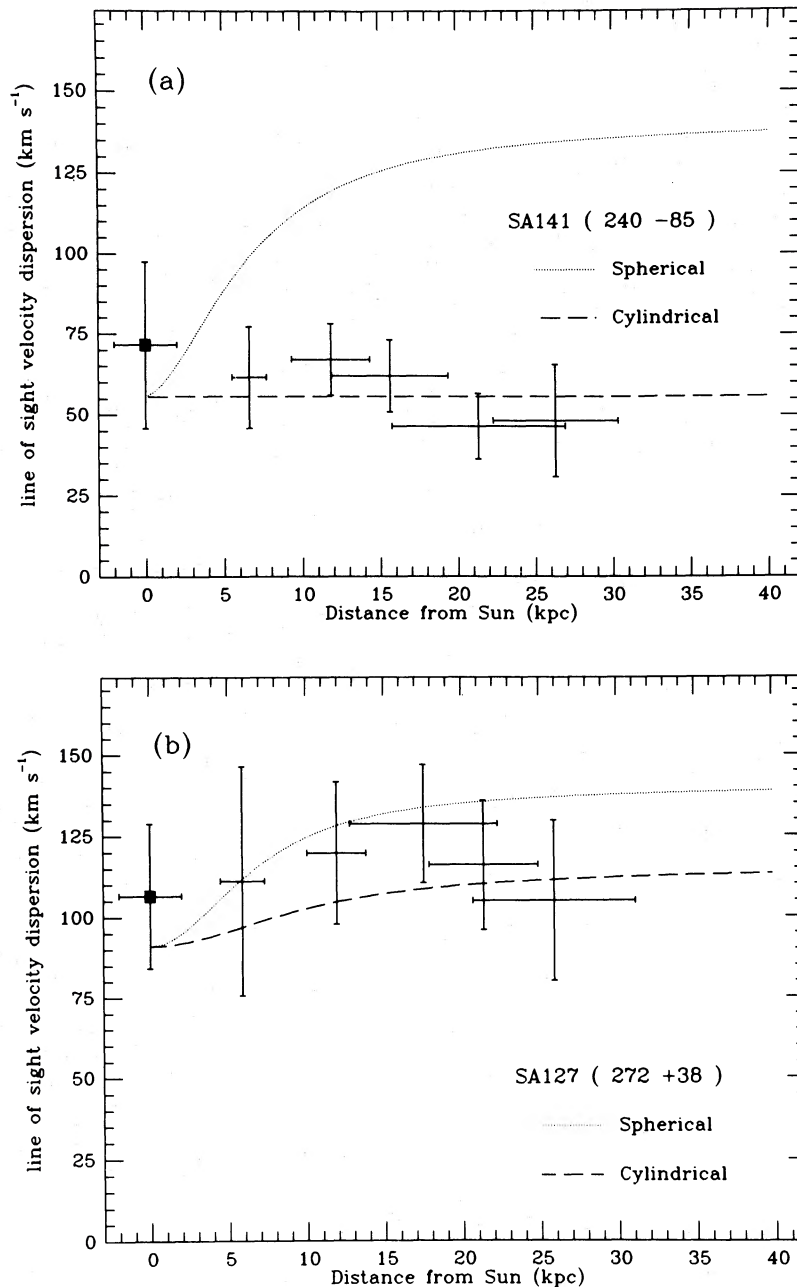


FIG. 3.—Line-of-sight velocity dispersions for subsamples (see text) of all the halo K giants in our fields (a) SA 141 and (b) SA 127 are shown plotted against distance. The expected run of σ_{los} is plotted assuming, in spherical and cylindrical polar coordinate systems, that the velocity ellipsoid remains constant and equal to the solar neighborhood values as estimated by Hartwick (1983) from 52 nearby metal-weak giants. Note that the spherical hypothesis, although consistent with observations in SA 127, is inconsistent with the low velocity dispersion seen in SA 141.

3a are dispersions about a zero mean. In the case of SA 127, the mean velocity of each subsample is not known *a priori*, so the velocity dispersions shown in Figure 3b are dispersions about the mean for each subsample. The error bars represent the dispersion about the mean distance and the standard error of the velocity dispersion for each subsample. Each star (except the most distant star in SA 127) appears in at least one sample. Most stars appear in more than one sample, so the data points in Figure 3 are not entirely independent. They do, however, represent the trend of velocity dispersion with distance.

We also show in Figure 3 a single point that represents the

σ_{los} that would be observed, in the directions of our fields, for a nearby population with the velocity dispersion (145, 124, 71) km s⁻¹ derived by Woolley (1978) for metal-weak RR Lyrae stars. Woolley's value is obviously consistent with Hartwick's estimate for the nearby giants, as used to calculate the predicted σ_{los} .

From Figure 3, we see that either hypothesis is consistent with the data for SA 127. However, the low velocity dispersion in the SGP field SA 141 is clearly inconsistent with the assumption that the velocity ellipsoid is everywhere elongated toward the galactic center (spherical hypothesis). Our alternative

hypothesis, of spatially uniform velocity dispersion components in cylindrical coordinates, gives a good representation of the data.

c) Other Halo Samples

There are several other halo samples that we can check against these hypotheses (see Table 3). Pier's (1982, 1983) data for halo BHB stars give a few more fields. We have grouped Pier's data in the following way to make up several galactic fields, each containing at least 20 stars. First, we estimated photometric parallaxes from his photometry, assuming the absolute magnitude-color relationship for the horizontal branch of M3. Most of Pier's stars lie between 2 and 10 kpc from the Sun. We excluded stars with distances less than 4 kpc, to derive velocity dispersion estimates independent of the solar neighborhood. For the first field, at the SGP, we have included only the 23 BHB stars with $|b| > 81$, to avoid contamination of σ_z by components of the motion parallel to the galactic plane. Next, there is an anticenter field at ($l = 186^\circ$, $b = -53^\circ$) and then three fields toward the galactic center, at latitudes $b = -57^\circ$, -28° , and -17° . Finally, we have combined the rotation fields near $l = 90^\circ$ and 270° , $b = -60^\circ$ to derive a single velocity dispersion value, making use of the obvious antisymmetry. Our data for SA 189 ($l = 277^\circ$, $b = -50^\circ$), while insufficient for detailed analysis, give another halo sample. Note the excellent agreement of σ_{los} for Pier's field (Pier f in Table 3) and our SA 189 field, which have similar (l , b) but different distances.

The number of stars, mean galactic coordinates, mean distances, and line-of-sight velocity dispersions σ_{los} , corrected for quoted measuring errors, are given in Table 3 for these samples. We will compare these values of σ_{los} with the line-of-sight velocity dispersion predicted under the two hypotheses described above. These predicted dispersions were calculated for each field, using the individual distances to each star, and are given in the last two columns of Table 3.

Figure 4 shows the predicted dispersion, under the two hypotheses, against the observed dispersion for these seven fields. Our hypothesis of constant velocity dispersion components in cylindrical coordinates (Fig. 4a) is apparently consistent with all the available velocity dispersion data for nonkinematically selected halo stars. Our alternative hypothesis of constant velocity dispersion components in spherical coordinates is clearly not consistent with the data shown in Figure 4b. The fields which give the best discrimination between the two hypotheses are the SGP field and the fields toward $l = 0^\circ$ at intermediate latitude (Pier c and Pier d). At the SGP, the line of sight lies along the minor axis of the velocity ellipsoid in the cylindrical hypothesis and approaches

the major axis for distant fields in the spherical hypothesis. On the other hand, for fields toward $l = 0^\circ$ and intermediate latitude and with distances of about 6 kpc from the Sun, the line of sight lies along the minor axis of the velocity ellipsoid in the spherical hypothesis: hence the low predicted σ_{los} for these fields.

We present the cylindrical hypothesis only as a simple working picture that appears to fit all the velocity dispersion data for halo stars, from a galactocentric distance of 3 kpc out through the solar neighborhood to a distance of at least 25 kpc from the Sun. Clearly, there is a large range of more complicated models that could represent the available velocity dispersion data for the halo stars. For example, although the data are inconsistent with the hypothesis of strict constancy of σ in spherical coordinates, the large discrepancies for the fields near $l = 0^\circ$, seen in Figure 4b, would disappear if the minor axis of the velocity ellipsoid were allowed to increase toward the galactic center. However, we cannot account for the small velocity dispersion observed at the SGP in this way.

d) The Circular Velocity

Our samples of distant giants at intermediate galactic latitudes can also be used to estimate galactic rotation, using standard procedures (Frenk and White 1980). Assuming a value for either the circular velocity V_0 at the Sun, or the systemic rotation of the outer galactic halo, it is possible to determine the other.

Consider the 22 more distant ($z > 10$ kpc) giants in the SA 127 and SA 189 fields. Assuming a zero mean rotation velocity for the outer halo gives a value of $V_0 = 212 \pm 34$ km s $^{-1}$; assuming a rotation velocity of about $+60$ km s $^{-1}$ (similar to that of the globular clusters) leads to an estimate $V_0 = 241 \pm 34$ km s $^{-1}$. These results are close to the generally accepted value of 220 km s $^{-1}$ for the circular velocity at the Sun; they show that our distant halo sample belongs to a slowly rotating population.

It is interesting to compare these estimates of mean rotation with those for the nearby kinematically selected samples. These samples give $\langle V \rangle = 192 \pm 13$ km s $^{-1}$ (Sandage 1969) and LSR, toward $l = 90^\circ$, $b = 0^\circ$. The close correspondence of these values suggests that the V -motions, at least, are not biased significantly by the kinematic selection.

In estimating the circular velocity from our data in SA 127, and also in our discussion of the velocity dispersion in §§ IVa and IVb, we have assumed that the distant stars come from a single kinematical population. However, inspection of Figures 1b and 2b suggests that this may not be so: to the eye, the stars appear bimodal in velocity, with one mode near 50 km s $^{-1}$ and the other near 250 km s $^{-1}$. Statistical tests on the velocities of

TABLE 3
COMPARISON OF MODELS

SAMPLE	NO. OF STARS	l (deg)	b (deg)	$\langle d \rangle$ (kpc)	OBSERVED	PREDICTED	
					σ_{los} (km s $^{-1}$)	σ_{sph} (km s $^{-1}$)	σ_{cyl} (km s $^{-1}$)
Pier a	23	78	-85	6.6	61 ± 9	94	56
Pier b	21	186	-53	5.8	110 ± 17	122	95
Pier c	26	1	-57	6.0	89 ± 12	63	89
Pier d	32	0	-28	6.4	116 ± 15	74	126
Pier e	36	2	-17	6.5	112 ± 13	94	133
Pier f	20	86/266	-54	6.7	83 ± 13	107	80
SA 189	16	276	-50	13.6	84 ± 15	125	89

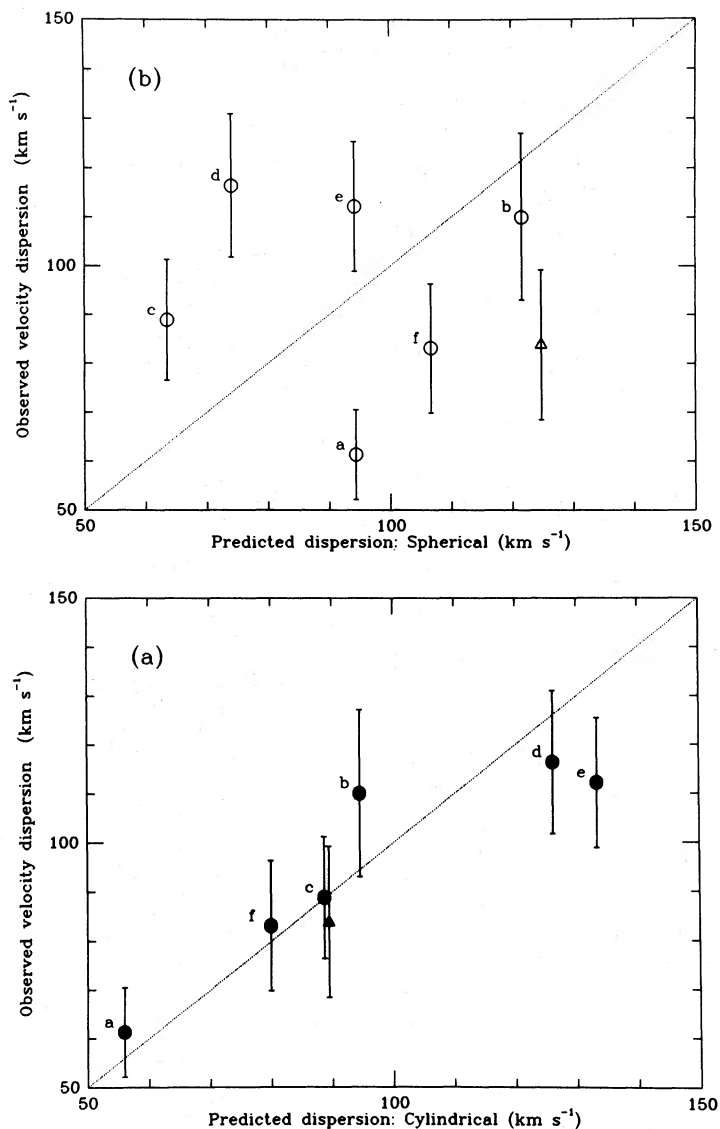


FIG. 4.—The observed velocity dispersions for Pier's fields designated a to f in Table 3 are shown plotted against the expected dispersions under the assumption that the velocity ellipsoid remains constant in (a) cylindrical and (b) spherical coordinates. See text for details. The triangle corresponds to our data for SA 189. The dotted line represents equality. Again, the cylindrical case gives a much better representation of the velocity dispersions in these halo fields.

the 39 stars in SA 127 show that their distribution *does not differ significantly* from a single Gaussian. However, if we were to take this apparent bimodality seriously, then the low-velocity mode would represent a rapidly rotating metal-weak component of the halo, while the high-velocity mode would correspond to a retrograde star stream (unless $V_0 > 330$ km s⁻¹). Both modes would be relatively cold ($\sigma_{\text{los}} \approx 50$ km s⁻¹). The possibility of a retrograde stream of metal-weak stars is reminiscent of the suggestion by Rodgers and Paltoglou (1984) on the origin of globular clusters with apparently retrograde orbits. At this stage, however, our evidence for this stream is weak, and would raise more problems than we wish to discuss here about the dynamics and structure of the halo.

V. DISCUSSION

We have described our survey for distant halo K giants, and have presented results on their kinematics. The main points are the following.

1. The outer halo is at most slowly rotating.
 2. The velocity dispersion for halo giants at the SGP (60 km s⁻¹) is approximately constant from the solar neighborhood to z -distances of about 25 kpc. It is much less than the velocity dispersion in the intermediate-latitude field SA 127: this is again constant with distance, at about 124 km s⁻¹.
 3. Our data on the run of velocity dispersion with distance for the outer halo giants is well represented by a simple kinematical model, in which the components (σ_R , σ_ϕ , σ_z) of the velocity dispersion in cylindrical polar coordinates remain constant everywhere. This model is also an excellent fit to Pier's (1983) kinematical data for BHB stars in the inner halo.
- Although our observed value for the z -dispersion of the distant halo K giants at the SGP (60 ± 8 km s⁻¹) may seem surprisingly low, it is consistent with other halo samples selected on nonkinematical criteria. Woolley (1978) finds 71 ± 26 km s⁻¹ for the nearby metal-weak RR Lyrae stars, and Hartwick (1983) derived 55 ± 31 km s⁻¹ for the nearby halo giants.

For Hartkopf and Yoss's (1982) sample of 23 metal-weak G and K giants at the galactic poles, with $\langle |z| \rangle = 4.3$ kpc, the dispersion is 51 ± 8 km s⁻¹. Pier's SGP sample at $(z) = 7$ kpc (Pier a in Table 3, with $\sigma_{\text{los}} = 61 \pm 9$ km s⁻¹) also agrees well with our value. The only other sample of distant halo stars at the galactic poles is the RR Lyrae stars at the NGP (Butler, Kinman, and Kraft 1979). Their systemic velocities are, however, more difficult to measure because of atmospheric effects. It will be interesting to see whether their kinematics show the same low dispersion as our field K giants. The measurements will need to be done to an accuracy of at least ± 20 km s⁻¹, with proper corrections for internal velocity variations, if a dispersion of 60 km s⁻¹ is to be measured from the observations.

Our value for the z -dispersion of the halo giants is, however, significantly lower than the value of 98 ± 7 km s⁻¹ for nearby kinematically selected metal-weak stars in the same abundance range (Eggen 1979; see also Sandage 1969). The reason for this difference between the nearby kinematically selected sample and the *in situ* nonkinematically selected samples (nearby and more distant) is not as yet clear. Presumably both samples come from the same metal-weak population. Proper dynamical models will be needed to see whether the kinematic selection introduces a sufficient bias to explain the different velocity dispersions in the z -direction. We note that the velocity dispersions in the R -direction are similar for the kinematic and nonkinematic samples, at about 150 km s⁻¹ (see Hartwick 1983; Eggen 1979).

Some extensions of this survey are planned. Another SGP field will be studied to improve on the statistics of the more distant giants in this field, which is so important for constraining the shape and orientation of the velocity ellipsoid. A distant field toward the anticenter will also be surveyed: this will show us directly whether the radial component of the

velocity dispersion remains constant with distance. Finally, although our data strongly suggest that the velocity dispersion σ is everywhere anisotropic in the halo, we do not of course have direct measurements of more than one component of σ at any place. For example, we have a value of σ_z at the SGP ($R = 8.5$ kpc, $z = 14$ kpc), and it would be very helpful to know σ_R and σ_ϕ at the same location. There is no immediate prospect of obtaining this information. However, it would be almost as good to have an estimate of σ_R and σ_ϕ at another location in the Galaxy, with the same (R, z) values. For example, at $l = 0^\circ$, $b = -39^\circ$, the line of sight passes through ($R = 8.5$ kpc, $z = 14$ kpc), at a distance of 22 kpc from the Sun: σ_{los} samples primarily the radial component of the velocity ellipsoid at this location. We plan to survey this field.

The apparent large-scale anisotropy of the velocity dispersion has interesting implications for the orbits of stars in the galactic halo, and therefore for the dynamical equilibrium and origin of the galactic halo itself. This is outside the scope of the present paper; we hope to discuss the dynamical consequences of the observed anisotropy in a later paper.

We are very grateful to John Bahcall, Michael Bessell, James Binney, Michael Fall, Martin Schwarzschild, Scott Tremaine, Tjeerd van Albada, and Simon White for discussions and advice, and to John Norris, who kindly allowed us to use his unpublished data. We are particularly grateful to ESO and to Dr H. E. Schuster, and to the UKSTU for the excellent Schmidt plates taken for this survey. We also thank the Anglo-Australian Observatory for their support during the spectroscopic observations. This work was mostly done while Ratnatunga held an Australian National University Ph.D. Scholarship, and was completed while we were both members of the Institute of Advanced Study, Princeton. Our thanks go to both institutions.

REFERENCES

- Bessell, M. S., and Norris, J. N. 1984, *Ap. J.*, **285**, 622.
 Bok, B. J., and Basinski, J. 1964, *Mem. Mt. Stromlo Obs.*, No. 16.
 Bond, H. E. 1980, *Ap. J. Suppl.*, **44**, 517.
 Burstein, D., and Heiles, C. 1982, *A.J.*, **87**, 1165.
 Butler, D., Kinman, T. D., and Kraft, R. P. 1979, *A.J.*, **84**, 993.
 Carignan, C. 1982, Ph.D. thesis, Australian National University.
 Clark, J. P. A., and McClure, R. D. 1979, *Pub. A.S.P.*, **91**, 507.
 Eggen, O. J. 1979, *Ap. J.*, **229**, 158.
 Eriksson, P.-I. W. 1978, *Uppsala Astr. Obs. Rept.*, No. 11.
 Frenk, C. S., and White, S. D. M. 1980, *M.N.R.A.S.*, **193**, 295.
 Hartkopf, W. I., and Yoss, K. M. 1982, *A.J.*, **87**, 1679.
 Hartwick, F. D. A. 1983, *Mem. Soc. Astr. Italiana*, **54**, 51.
 Jeans, J. H. 1916, *M.N.R.A.S.*, **76**, 70.
 Kraft, R. P. 1979, *Ann. Rev. Astr. Ap.*, **17**, 309.
 Morgan, W. W., Keenan, P. C., and Kellman, E. 1943, *MKK Yerkes Atlas* (Chicago: University of Chicago Press).
 Norris, J. E. 1983, private communication.
 Norris, J. E., Cottrell, P. L., Freeman, K. C., and Da Costa, G. S. 1981, *Ap. J.*, **244**, 205.
 Norris, J. E., and Freeman, K. C. 1983, *Ap. J.*, **266**, 130.
 Norris, J. E., Freeman, K. C., and Da Costa, G. S. 1983, *Ap. J.*, **277**, 615.
 Norris, J. E., and Zinn, R. 1977, *Ap. J.*, **215**, 74.
 Pier, J. R. 1982, *A.J.*, **87**, 1515.
 ———. 1983, *Ap. J. Suppl.*, **53**, 791.
 Ratnatunga, K. U. 1982, *Proc. Astr. Soc. Australia*, **4**, 422.
 ———. 1983, Ph.D. thesis, Australian National University.
 ———. 1984, in preparation.
 Ratnatunga, K. U., and Freeman, K. C. 1983, *IAU Colloquium 78, Astronomy with Schmidt-Type Telescopes* (Dordrecht: Reidel), p. 261.
 Richstone, D. O. 1980, *Ap. J.*, **238**, 103.
 Rodgers, A. W., and Paltoglou, G. 1984, *Ap. J. (Letters)*, **283**, L5.
 Saha, A. 1984, Ph.D. thesis, California Institute of Technology.
 Sandage, A. 1969, *Ap. J.*, **158**, 1115.
 Woolley, R. 1978, *M.N.R.A.S.*, **184**, 311.

K. C. FREEMAN: Mount Stromlo and Siding Spring Observatories, Private Bag, Woden, P.O. ACT 2606, Australia

KAVAN U. RATNATUNGA: Institute for Advanced Study, Princeton, NJ 08540